

# Compact expansion of a repulsive suspension

Matan Yah Ben Zion<sup>1</sup> and Naomi Oppenheimer<sup>1, \*</sup>

<sup>1</sup>*School of Physics and the Center for Physics and Chemistry of Living Systems, Tel Aviv University, Tel Aviv 6997801, Israel*  
(Dated: March 1, 2023)

We find that a suspension of particles that mutually repel by short-ranged interactions spreads compactly. Unlike the diffusive boundary of a spreading drop of Brownian particles, here, the density is strictly zero beyond a cutoff distance. We identify that the drop expands in a self-similar fashion in the dense limit. Starting from the pair potential, we show that in the continuum limit, the suspension's expansion follows a nonlinear diffusion equation. At early times (dense limit), the density profile is parabolic, and the area of the ensemble grows as the square root of time. At later times (sparse limit), the dynamics slow down and transition to a logarithmic growth. We verify the approximations of the analytical predictions in the dense regime using exact numerical integration. We examine the dilute regime by monitoring the expansion of a charged stabilized colloidal suspension and find the logarithmic expansion is consistent with the experiment. Using molecular dynamics simulation of thousands of particles, we see the crossover between the two regimes as the dynamics transition from self-similar to logarithmic.

Colloidal suspensions are everywhere — from the ink we (used to) write with, the soy milk we drink and the drugs we consume, to the very structure of most living systems. Life is built of microscopic particles suspended in a fluid. More often than not the particles are charged and the electrostatic interactions are screened by the presence of ions in solution [1, 2]. Such is the case for charged proteins in a membrane [3–6], vesicles in suspension [7], droplets in microfluidic devices [8], water purification, and plasma physics [9, 10]. In other cases, particles are not strictly charged, yet are repelled by short-range forces, e.g. globular polymers, or colloidal particles coated by a brush shell, and sub-atomic particles interacting in the nucleus [11–13].

In what follows, we consider the expansion of a suspension of particles with repulsive, short range interactions that dominate over thermal diffusion. We find that when the interaction has a typical decay length, the suspension expands compactly — the concentration vanishes identically outside a core of finite size. Compact profiles are found in diverse physical systems including gas diffusion through porous medium [14, 15], thin films with a free surface [16, 17], and even in population dynamics [18]. A family of compact solitons (called compactons) were found as solutions to a generalization of the Korteweg-De Vrie (KdV) equation [19]. These systems were modeled using a continuum, hydrodynamic description, characterized by phenomenological parameters. Here we show analytically, starting from a microscopic basis, that a non-linear diffusion equation with a compact solution is generic for particles with short range repulsion. We find under what conditions the continuum description breaks down, leading to a crossover in the dynamics.

As we outline below, at high densities, the time evolution and distribution of the density field  $n(\mathbf{r}, \mathbf{t})$ , are determined by a non-linear diffusion equation, stemming from particle interactions, leading to a concentration de-

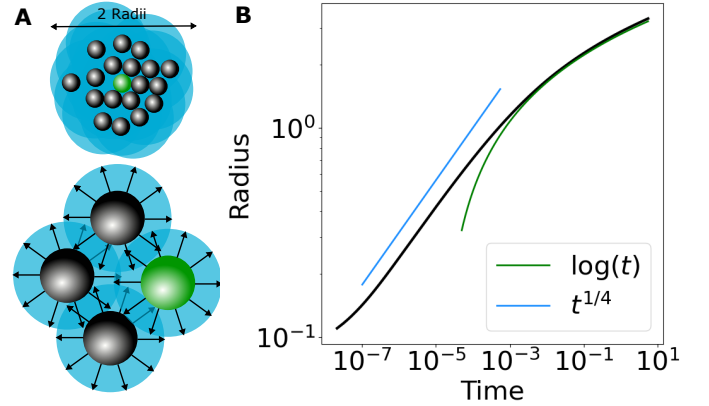


FIG. 1. (a) Schematics of the interaction of repulsive particles with short-range repulsion in the dense region (top), where each particle interacts with many others, and in the sparse region (bottom), where a particle interacts only with its nearest neighbors. (b) MD simulation of 10,000 particles starting from a dense random distribution. At early times we see the  $R \sim t^{1/4}$  scaling predicted by the self-similar solution. At long times there is a transition to the sparse limit with a logarithmic dependence on time.

pendent diffusion of the form

$$\frac{\partial n}{\partial t} = \nabla [D(n)\nabla n] = D(n)\nabla^2 n + \alpha|\nabla n|^2, \quad (1)$$

with  $D(n) = \alpha n$ , and we derive  $\alpha$  from the microscopic pair potential. Since the effective diffusion coefficient,  $D(n)$  is proportional to the density, particles at the drop's boundary have a lower diffusion constant than particles at the edge. The solutions are inherently different from regular diffusion. For example, for diffusion, there is a Gaussian spread of the density. Here, the density profile is parabolic and is strictly zero beyond a maximal radius which grows with time. Unlike classic diffusion, here, the area of the drop does not grow linearly with time but as the square root of time. At lower densities, when the dis-

tance between particles is larger than the characteristic repulsive distance, particle interactions are dominated by nearest neighbors. We show that in this limit, the suspension spreads logarithmically with time.

The expansion of the repulsive suspension can be described by the time evolution of its radius. For exponential or screened electrostatic interactions, the asymptotic limits of the time evolution are given by

$$R(t) \propto \begin{cases} t^{1/4} & \text{if } n \gg 1 \\ \log(t) & \text{if } n \ll 1 \end{cases}, \quad (2)$$

where  $n = \rho/\rho_c$  is the non-dimensionalized density,  $\rho_c = 1/(\pi l^2)$ , with  $l$  being the typical decay of the short-range repulsion. The transition from the two types of expansions occurs when the typical distance between particles,  $L$  is equal to the decay length,  $l$ . Our analysis addresses the athermal limit, where Brownian motion is negligible. This is valid when  $D = \alpha n \gg D_0$  where  $D_0$  is the self diffusion coefficient originating from thermal fluctuations. Similarly, this is true when the distance between particles satisfies  $L \ll \sqrt{2\pi F_0 l^3/k_B T}$ , where  $F_0$  is the strength of the repulsive force,  $k_B$  is Boltzmann constant, and  $T$  is temperature. Note that in the over-damped dynamics discussed here, this limit is independent of viscosity, which plays a dual role in both the deterministic and stochastic forces.

Equations 1 and 2 are the main results of this work, which is structured as follows: first, we derive the two regimes analytically. Next, we compare analytic results with simulations and experiments. We show that at high densities ( $n \gg 1$ ), both numerical integration of the mass conservation equation, as well as Molecular Dynamics (MD) simulations using the pair interactions, are quantitatively consistent with the approximate analytical solution; then we proceed to show that the low density limit ( $n \leq 1$ ) indeed follows Eq. 2 as observed in both experiments of a concentrated charged colloidal suspension and MD simulations.

## GOVERNING EQUATIONS

We examine particles in the overdamped limit, where inertia is negligible, and the force,  $\mathbf{F}$  and velocity  $\mathbf{v}$ , are proportional through constant mobility,  $\mathbf{v} = \mu\mathbf{F}$ . Individual particles follow deterministic dynamics (no Brownian motion) and interact through a pair interaction,  $F(r)$ . The interaction can be due to any short-ranged, isotropic, repulsive force — from sub-atomic Yukawa potential, through Pauli repulsion at the inter-atomic scale, screened Coulomb potential in an ionic solution or plasma, or even soft-core entropic repulsion in colloidal suspensions [10, 11, 20–22]. Our results are generic, but for simplicity, we consider exponential interactions in the

main text,  $F(r) \sim e^{-r/l}$ . In the Supplementary Information (SI), we show results for screened-electrostatics.

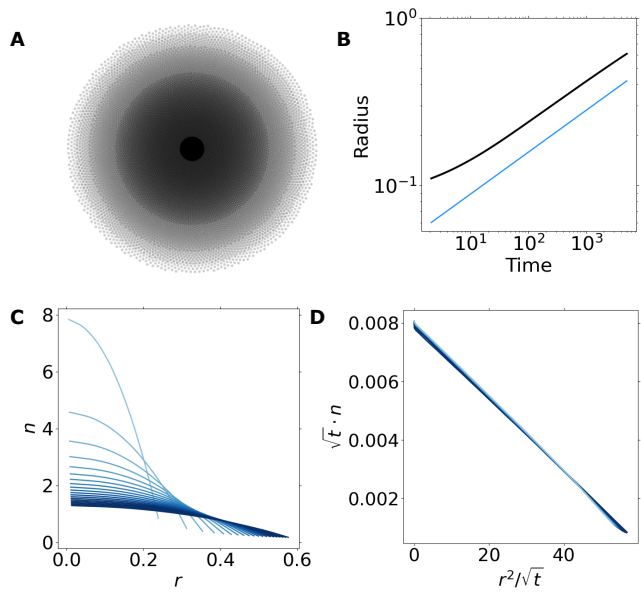


FIG. 2. Molecular dynamics simulations of repulsive particles at high density show self-similar profile, as predicted in the continuum limit. Results from a simulation of 10,000 particles with exponentially repulsive interactions. We start from a high density and track the particles as they spread. a) Snapshots of the simulations at different times ( $t = 0, 5, 000, 20, 000, 35, 000, 50, 000$ ). b) Radius as a function of time showing an the  $t^{1/4}$  scaling. c) Density as a function of radius for different times. Color goes from bright to dark as time progresses. d) Re-scaled density  $\sqrt{t} \cdot n$  as a function of  $r^2/\sqrt{t}$  showing all the curves collapse to a single one as predicted by Eq. 12.

To build intuition, let us start by examining a single particle, then two, and then many. For a single Brownian particle, the mean-square displacement grows as  $\sqrt{t}$ . By contrast, a single repulsive, athermal particle, is stationary. Unlike the separation between two Brownian particles that diffuse apart at a rate of  $\sqrt{t}$ , two athermal, strictly repulsive particles separate as  $\sim \log(t)$  since  $dr/dt = v_0 e^{-r/l}$ , where  $v_0$  is the magnitude of the velocity given by  $v_0 = \mu F_0$ . In the ensemble limit, the area of  $N$  diffusing particles grows as  $\sqrt{t}$ . Repulsive particles move due to the sum of the interaction from all their neighbors. That is, the velocity of particle  $i$  is given by,

$$\mathbf{v}_i(\mathbf{r}_i) = - \sum_j v_0 e^{-\frac{|\mathbf{r}_i - \mathbf{r}_j|}{l}} \frac{\mathbf{r}_i - \mathbf{r}_j}{|\mathbf{r}_i - \mathbf{r}_j|}, \quad (3)$$

Molecular dynamic simulations of Eq. 3 (see Fig. 1) show that an ensemble of  $N$  repulsive particles grows as  $R \sim t^{1/4}$  in the dense limit ( $n \gg 1$ ) and as  $\log(t)$  in the dilute limit ( $n \leq 1$ ), that is — (a) subdiffusively, and (b) similar to the spread of two repulsive particles in the dilute limit but very differently than the dense limit.

When does the two particle case transition to the continuum description? We will now derive analytically the cross-over between these two limits.

**Analytic Results in the Dense Limit.** In the dense limit,  $n \gg 1$ , we coarse-grain the velocity to derive a diffusion equation. The following procedure is analogous to a Focker-Planck expansion with a mean-field closure [23–26]. We start with the mass conservation equation for the number of particles

$$\frac{\partial n}{\partial t} + \nabla \cdot (n\mathbf{v}) = 0, \quad (4)$$

where  $n$  is the normalized density of particles such that  $n = \rho/\rho_c$ ,  $\rho(\mathbf{r}(t)) = \sum_i \delta(\mathbf{r}(t) - \mathbf{r}_i(t))$ , and  $\rho_c = 1/(\pi l^2)$  is the critical density. We turn to find the coarse-grained velocity,  $\mathbf{v}(\mathbf{r}(t))$ . Since the interactions are purely repulsive, the velocity field is of the form  $\mathbf{v}(\mathbf{r}) = v(r)\hat{r}$  [27], where  $v(r)$  is given by the short-ranged repulsive force felt from all other particles. In the limit of a continuous density of particles, Eq. 3 becomes

$$\mathbf{v}(\mathbf{X}) = -v_0 \rho_c \int_0^R \int_0^{2\pi} n(\mathbf{Y}) \frac{\mathbf{X} - \mathbf{Y}}{|\mathbf{X} - \mathbf{Y}|} e^{-\frac{|\mathbf{x}-\mathbf{y}|}{l}} d^2\mathbf{Y} \quad (5)$$

Equation 5 combined with the mass conservation, Eq. 4, can be solved numerically, as we show later on. To continue analytically, we must turn to approximations.

In principle, the integration boundaries depend on the position of the particle  $\mathbf{X}$ , but distances  $|\mathbf{X} - \mathbf{Y}| \gg l$  will hardly contribute due to the short-ranged nature of the forces. For particles away from the edge of the suspension,  $|R - X| \gg l$ , we can extend the integration boundaries to the entire space. Thus the velocity is approximately

$$\mathbf{v}(\mathbf{X}) \approx -\frac{v_0}{\pi} \int_0^\infty \int_0^{2\pi} n(\mathbf{X} + l\mathbf{s}) \frac{\mathbf{s}}{s} e^{-s} d^2\mathbf{s}, \quad (6)$$

where we have changed integration variables to a normalized distance  $\mathbf{s} = (\mathbf{Y} - \mathbf{X})/l$ . In polar coordinates  $\mathbf{s} = r(\cos\theta, \sin\theta)$ ,  $\mathbf{X} = r'(\cos\phi, \sin\phi)$ , with  $\theta \in (0, 2\pi)$  and  $s \in (0, \infty)$ . We do a multipole expansion of Eq. 6 by expanding the density in a Taylor series,

$$n(\mathbf{X} + l\mathbf{s}) \approx n(\mathbf{X}) + l\mathbf{s} \cdot \nabla n(\mathbf{X}) + \dots \quad (7)$$

By symmetry, the first term of the moment expansion in Eq. 7 vanishes after integration in Eq. 6 (odd integrand over an even domain). The remaining leading term in the velocity is the concentration gradient,

$$\mathbf{v}_r(\mathbf{X}) \approx -\frac{lv_0}{\pi} \nabla n(\mathbf{X}) \cdot \int \mathbf{s} \hat{s} e^{-s} d^2\mathbf{s} = -\alpha \frac{\partial n}{\partial r} \hat{r}, \quad (8)$$

with  $\alpha = 2v_0l/\pi$ . More generally  $\alpha = \frac{\rho_c}{\mu} \int \mathbf{r} \cdot \mathbf{F}(r/l) d^2r$ , where  $\mathbf{F}(r/l)$  is the short-ranged force. For example, screened electrostatic interactions have the potential  $U = U_0l \exp(-r/l)/r$ , and the velocity will have

the form  $v = -v_0l/r \exp(-r/l) - v_0l^2/r^2 \exp(-r/l)$ , with  $v_0 = \mu U_0/l$ . The result is then  $\alpha = 3v_0l/\pi$ , changing only the pre-factor of the exponential case by 3/2. We show simulation results for such a case in the SI.

The full non-linear diffusion equation (Eq. 1) is found when plugging the velocity approximation (Eq. 8) in the equation for mass conservation (Eq. 4), giving an effective diffusion coefficient that linearly increases with density,  $D = \alpha n(r)$ , which takes the following form in polar coordinates:

$$\frac{\partial n}{\partial t} - \frac{\alpha}{r} \frac{\partial}{\partial r} \left( r n \frac{\partial n}{\partial r} \right) = 0. \quad (9)$$

This equation is identical to the effective porous media equation [14] but derived from the details of the pair interaction, allowing us to trace the effective parameters to their microscopic origins. Self-similar solutions are given by dimensional analysis of Eq. 9 (see Refs. [16, 17]). We start by assuming a solution of the form  $n = At^\gamma f(Br/t^\beta) = At^\gamma f(\eta)$ . We can further link  $\gamma$  and  $\beta$  by recalling that the total number of particles,  $N$ , is independent of time

$$N = \rho_c \int n(r) r dr d\theta \propto t^{\gamma+2\beta} \int f(\eta) \eta d\eta. \quad (10)$$

which is constant only for  $\gamma = -2\beta$ . The density therefore has the form  $n = At^{-2\beta} f(Br/t^\beta)$ . Placing  $n$  in Eq. 9, we find that  $f$  is indeed a function of  $\eta$  alone (as was assumed), and we must have  $\beta = \frac{1}{4}$ , and  $B^2 = \frac{1}{8A\alpha}$ . The equation for the self-similarity function,  $f$ , is

$$2f + \eta f' = -\frac{1}{2\eta} \frac{d}{d\eta} (\eta f f'), \quad (11)$$

whose solution is parabolic, such that the concentration is

$$n = \frac{A}{\sqrt{t}} (1 - \eta^2) = \frac{A}{\sqrt{t}} \left( 1 - B^2 \frac{r^2}{\sqrt{t}} \right). \quad (12)$$

Finally, the prefactor,  $A$ , is determined from the total number of particles (Eq. 10), giving  $A = \sqrt{3N/(8\pi\rho_c\alpha)}$ . The self-similar profile is quadratic with respect to  $\eta$  hence it is quadratic with respect to distance, and its width is an increasing function of time. Note that the concentration of particles is *strictly zero* beyond  $r = t^{1/4}$ , meaning that the drop is compact.

**Analytic Results in the Sparse Limit.** When the average distance between particles is larger than the decay length of the repulsive force,  $l$ , we can assume only nearest neighbors contribute to the interaction, and the discrete nature of the suspension cannot be ignored. In such cases, we can no longer use Eq. 8 in order to find the density as a function of time. However, we can still approximate the radius of the drop as it spreads by considering the velocity of particles at the edge. Since in this

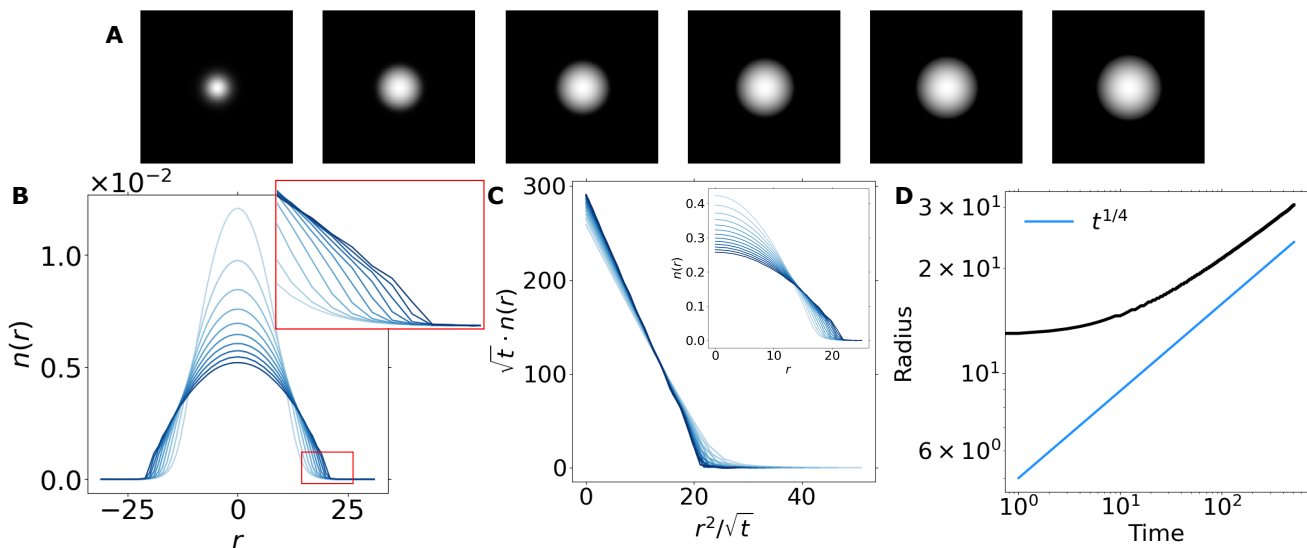


FIG. 3. Full numerical solution of Eq. 4 combined with Eq. 5 using Fast Fourier Transform with padded arrays. a) Snapshots of the density distribution at constant time intervals show that a repulsive suspension starting with an initially smooth Gaussian distribution spreads compactly. b) Radially averaged density profile as a function of the radius of the drop at different times. Inset shows a zoom-in on the edge of the drop, showing the sharpening of the cusp over time. Color goes from bright to dark as time progresses. c) Collapsed plot of the re-scaled distributions at later times (following Eq. 12). Density is scaled by  $\sqrt{t}$  and plotted against  $\eta = r^2/\sqrt{t}$  as predicted by Eq. 12 for the approximate velocity, Eq. 8. Inset shows a plot of the density versus distance used for the figure. d) Radius as a function of time showing the expected growth as  $t^{1/4}$ .

limit particles predominately interact with their nearest neighbors, their velocity can be readily approximated. Due to the repulsive interactions, the arrangement of particles is hexagonal. We can assume a particle at the edge of the drop has three equally spaced nearest neighbors. Due to the isotropic nature of the interactions we can consider any particle. Without loss of generality, we take the particle positioned at  $\mathbf{r} = R\hat{x}$ . The particle will move with velocity  $\mathbf{v}(R\hat{x}) = \frac{dR(t)}{dt}\hat{x} = 2v_0 e^{-R/\sqrt{N/\pi}l}\hat{x}$ , where  $R/\sqrt{N/\pi}$  is the average distance between particles in the ensemble. The approximate radius is simply found by integrating the velocity

$$R(t) = \sqrt{\frac{N}{\pi}} l \log(t/t_0 + c), \quad (13)$$

with  $t_0 = \sqrt{N/\pi}l/2v_0$  and  $c = \exp(\sqrt{R_0^2\pi/lN^2})$  where  $R_0$  is the initial radius. To test the validity of this result we ran MD simulations and experiments of a concentrated suspension of charge stabilized colloids in deionized water.

## DENSE LIMIT VERIFICATION

**Molecular Dynamics Simulation in the Dense Limit.** We ran simulations of 10,000 particles with short-ranged exponential repulsion. We start from a random configuration in a circle of size  $R$  and let the system

evolve over time using a 5<sup>th</sup> order Runge-Kutta scheme while adapting step size according to the distance between particles. As the drop evolves, it spreads, such that  $R = R(t)$ . We find the local density of particles by finding the Voronoi tessellation and calculating the area of each cell,  $A_{\text{cell}}^i$  [28]. The density is given by  $n(r) = 1/A_{\text{cell}}^i$ . The upper left panel in Fig. 2 shows overlaid snapshots from the simulation at different times. Figure 2B shows the radius of the drop as a function of time. After a short transient, indeed it follows the expected power-law of Radius  $\propto t^{1/4}$ . The density profile as a function of the radius of the drop,  $r$ , at different times is presented in Fig. 2C. And lastly, the bottom right panel shows the re-scaled density  $\sqrt{t}n$  versus  $\eta = r^2/\sqrt{t}$  excluding the first few timesteps. Note how at longer times, all the curves collapse to a single straight line according to the scaling of Eq. 12.

**Numerical Solutions in the Dense Limit.** To test the validity of the asymptotic solution, we have numerically integrated the mass conservation equation, Eq. 4 together with the full velocity given by Eq. 5. Note that this is a numerical solution of the *full* partial differential equations. That is, without resorting to any of the assumptions used to derive Eq. 6 and the nonlinear diffusion equation, Eq. 9. Namely, without the asymptotic approximation of the integral in Eq. 5, and using the full density distribution (not only the first nonvanishing term in its Taylor expansion). To that end, we started with a narrow Gaussian distribution with a standard devia-

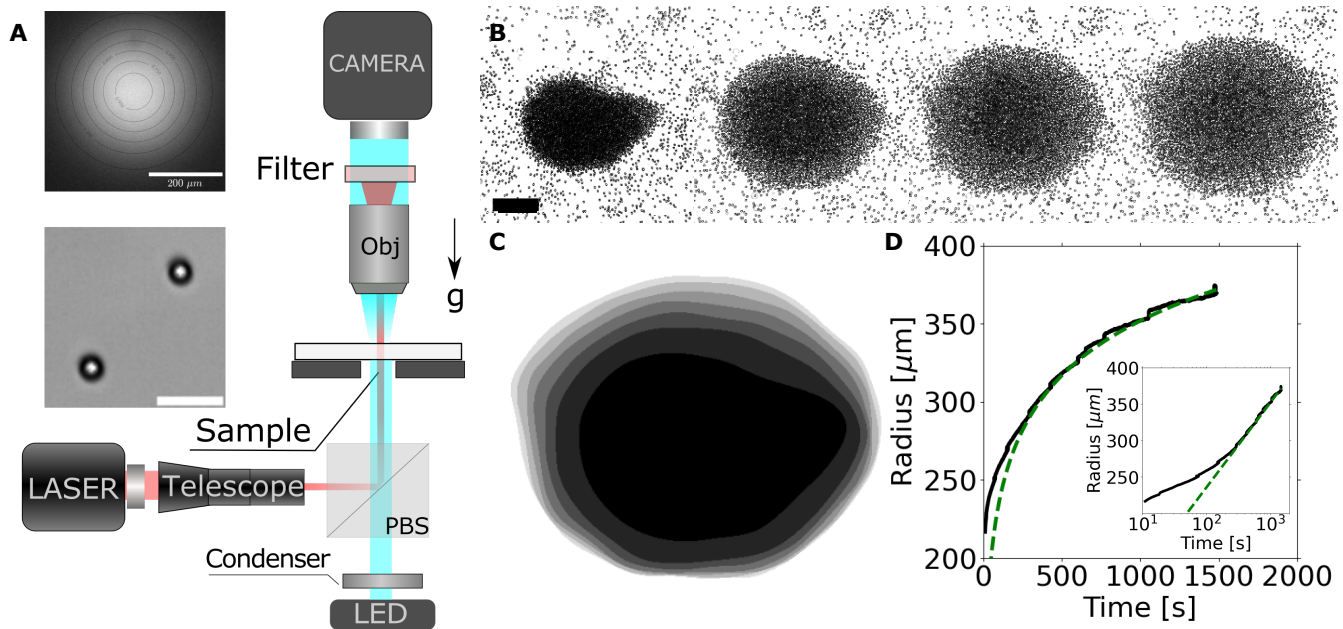


FIG. 4. Experimental results. (A) Large field optical tweezer setup. Top inset shows the light field intensity distribution of the image of the sample (Scalebar  $200 \mu\text{m}$ ). Bottom inset shows an image of two colloidal particles on the surface (Scalebar  $10 \mu\text{m}$ ). (B) Snapshots of a dense suspension with  $N \approx 10^4$  particles show a compact expansion, with particles spreading due to screened electrostatic repulsion. Scalebar  $100 \mu\text{m}$  (C) Overlapping figures with a color threshold (D) Drop radius as a function of time. The radius shows a logarithmic dependence (green dashed line) as predicted by the theory for a sparse suspension.

tion  $\sigma = 0.03$  on a grid of  $N \times N = 128 \times 128$ , and with a timestep  $dt = 1/N^2$ . In each time step, we calculated the velocity using convolution in Fourier space of Eq. 5 while making sure the convolution is well behaved by adding padded arrays. The spatial part of the partial differential equation was solved using FFT whereas the time integration scheme which was chosen is Leapfrog. We propagated the dynamics over  $t = 32,000$  timesteps. The numerical results are presented in Fig. 3. On the left bottom panel, the density as a function of radius is presented at various times. The inset shows a zoom-in on the edge of the drop, showing that at later times, a cusp is formed, indicating the compactness of the solution. In the bottom-middle panel, the normalized density  $\sqrt{t}n(r)$  is plotted as a function of  $\eta = r^2/\sqrt{t}$ , where a collapse of all later times to a single straight curve is obtained, as expected from the nonlinear diffusion Eq. 12. Lastly, on the right-bottom panel, the radius as a function of time shows the expected power-law of  $\propto t^{1/4}$ .

### SPARSE LIMIT VERIFICATION

**Experiments of the Expansion of a Colloidal Suspension.** We tested experimentally the expansion of a colloidal suspension by concentrating particles using optical tweezers, then turning off the light, and monitoring the spreading of the colloidal drop (see Fig. 4). Most commonly, optical tweezers have the laser light first en-

ter the objective rear, coming to a tight focus at the imaging plane [29]. This creates a strong, yet small trap, that can typically host a single colloidal particle ( $\sim 1 \mu\text{m}$ ). To make a trap that can tweeze many particles we built custom optical tweezers by using a nearly collimated laser beam that first passes through the sample (and only then enters the objective through the collecting lens) [30, 31]. For this a custom Galilean telescope was used to shrink a 3 mm IR laser source (1064 nm IPG Photonics) into a nearly collimated beam with a diameter of  $D \approx 300 \mu\text{m}$  at the sample (see Fig. 4A). We used  $d = 3 \mu\text{m}$  colloidal particles (Bangslabs) suspended in deionized water (Millipore,  $18.2\text{M}\Omega\text{cm}$ ), with  $\text{pH} \approx 6.3$ . The particles are charged stabilized, and repel through screened Coulomb interaction, and can be approximated using the DLVO theory to follow  $U(r) \propto \exp\{d/1-r/l\}/r$ , where  $l$  can be approximated from the Debye screening length,  $l \approx \lambda_D + d/2$ , where  $\lambda_D \approx 1\mu\text{m}$  [32]. The suspension was loaded into a  $100 \mu\text{m}$  tall, passivated capillary glass (Vitrotubes, see supporting information for treatment details). Particles settle at the bottom surface and form a quasi-2D suspension (gravitational height  $h_g \approx 20\text{nm} < 0.01d$ ) with a filling fraction of  $Nd^2/D^2 \lesssim 0.9$ . Note that the high filling fraction is still in the sparse limit, as  $l \lesssim d$ . With no light, individual particles display Brownian motion with a measured diffusion constant of  $D_0 = 0.11 \pm 0.02\mu\text{m}^2/\text{s}$  as measured from the mean square displacement of individually tracked particles (see Supporting Information).

When the laser is turned on, particles are softly attracted into the region of a higher optical field, collecting approximately  $N \approx 10^4$  particles (see Fig. 4A). Particles are packed at an effective area fraction of 0.9. Given the individual diffusion constant, and the effective area fraction, the suspension is expected to be in the dilute regime ( $n < 1$ ) described in Eq. 2, but above the diffusive regime. Once the beam is turned off, the suspension starts to spread. During the initial half hour of spreading, the suspension remains compact with a sharp boundary. At later times, the boundary turns diffusive and the expansion is no longer compact (see supporting Movie 1). We measure the size of the drop in the compact expansion regime by thresholding the movie (Fig. 4) and extracting the radius of the drop at each frame. We find that as predicted by Eq. 2, the suspension expands logarithmically.

**Molecular Dynamics Simulation in the Sparse Limit.** Running simulations of 10,000 either for very long times or starting from a sparse random configuration results in a logarithmic growth of the radius of the drop as a function of time. Figure 1 shows a transition from a  $R \sim t^{1/4}$  at early times, as predicted by the self similar solution, to  $\sqrt{N/\pi l} \log(t)$  as predicted in the sparse limit, Eq. 13. Even though the analytic arguments made rough assumptions, namely, taking the average distance between particles as a measure of spacing, the coefficient of the logarithm is correctly predicted. In our case  $l = 0.005$  giving  $\sqrt{N/\pi l} = 0.28$ .

**Conclusions.** We have characterized the compact expansion of a repulsive suspension using theory, numeric integration, simulations, and experiments. An ensemble of repulsive particles spreads in a subdiffusive manner — with a power law of  $t^{1/4}$  in the dense limit, when distance between particles is smaller than the decay length of the repulsive potential, and logarithmically in the sparse limit when particles only interact with their nearest neighbors. In our work we verified experimentally only the sparse limit, but the dense limit can also be accessed in a colloidal sample using recently recent protocols [33] where the screening length much exceeds the particle size. Our results link the microscopic pair potential to macroscopically observed dynamics in ensembles dominated by interactions.

**Author Contribution.** NO initiated the research, derived the theory, and developed the molecular dynamics simulations. MYBZ performed experiments. Both authors wrote the numerical integration code, analyzed the data, and wrote the manuscript.

**Acknowledgments.** We thank Michael Shelley, Haim Diamant, and Philip Rosenau for helpful discussions.

- [1] J. C. Crocker and D. G. Grier, *MRS Bulletin* **23**, 24 (1998).
- [2] C. N. Likos, *Physics Reports* **348**, 267 (2001).
- [3] J. J. Sieber, K. I. Willig, C. Kutzner, C. Gerding-Reimers, B. Harke, G. Donnert, B. Rammner, C. Eggeling, S. W. Hell, H. Grubmüller, *et al.*, *Science* **317**, 1072 (2007).
- [4] F. B. Sheinerman, R. Norel, and B. Honig, *Current opinion in structural biology* **10**, 153 (2000).
- [5] N. Oppenheimer, D. B. Stein, and M. J. Shelley, *Physical review letters* **123**, 148101 (2019).
- [6] B. Sorkin and H. Diamant, *Biophysical Journal* **120**, 2030 (2021).
- [7] T. H. Anderson, S. H. Donaldson, H. Zeng, and J. N. Israelachvili, *Langmuir* **26**, 14458 (2010).
- [8] D. R. Link, E. Grasland-Mongrain, A. Duri, F. Sarrazin, Z. Cheng, G. Cristobal, M. Marquez, and D. A. Weitz, *Angewandte Chemie International Edition* **45**, 2556 (2006).
- [9] J. Crow, P. Auer, and J. Allen, *Journal of Plasma Physics* **14**, 65 (1975).
- [10] J. P. Freidberg, *Cambridge University Press*, Vol. 1 (2007) p. 671, arXiv:arXiv:1011.1669v3.
- [11] A. Y. U. Grosberg and A. R. Khokhlov, *Statistical Physics of Macromolecules* (American Institute of Physics, 1994) p. 351.
- [12] S. Milner, T. A. Witten, and M. E. Cates, *Macromolecules* **21**, 2610 (1988).
- [13] H. D. Young, R. A. Freedman, and A. Lewis Ford, *University Physics with Modern Physics Technology Update: Pearson International Edition* (2013) p. 1744.
- [14] G. I. Barenblatt, *Prikl. Mat. Makh.* **16**, 67 (1952).
- [15] R. Pattle, *The Quarterly Journal of Mechanics and Applied Mathematics* **12**, 407 (1959).
- [16] H. Stone, in *Nonlinear PDE's in Condensed Matter and Reactive Flows* (Springer, 2002) pp. 297–312.
- [17] L. G. Leal, *Advanced transport phenomena: fluid mechanics and convective transport processes*, Vol. 7 (Cambridge University Press, 2007).
- [18] Z. Zhao, L. Li, and Z. Feng, *Mathematical Methods in the Applied Sciences* (2021).
- [19] P. Rosenau and J. M. Hyman, *Physical Review Letters* **70**, 564 (1993).
- [20] H. Yukawa, *Proceedings of the Physico-Mathematical Society of Japan. 3rd Series* **17**, 48 (1935).
- [21] P. Atkins, J. de Paula, and J. Keeler, *Atkins' Physical Chemistry 11th Edition*, 11th ed. (Oxford University Press, Oxford, 2018) p. 940.
- [22] P. M. Chaikin and T. C. Lubensky, *Principles of Condensed Matter Physics* (Cambridge University Press, 1995) p. 720.
- [23] B. U. Felderhof, *Journal of Physics A: Mathematical and General* **11**, 929 (1978).
- [24] D. S. Dean, *Journal of Physics A: Mathematical and General* **29**, L613 (1996).
- [25] N. Martzel and C. Aslangul, *Journal of Physics A: Mathematical and General* **34**, 11225 (2001).
- [26] M. Bruna, S. J. Chapman, and M. Robinson, *SIAM Journal on Applied Mathematics* **77**, 2294 (2017).
- [27] As a side comment, if the velocity has a rotational component such that  $\mathbf{v}(\mathbf{r}) = \mathbf{v}_r(\mathbf{r})\hat{r} + \mathbf{v}_\theta(\mathbf{r})\hat{\theta}$ , that is the rotational component of the velocity,  $\mathbf{v}_\theta = v_\theta(r)\hat{\theta}$  is solely a function of  $r$ , the rotational part is incompressible.

---

\* naomiop@gmail.com

- ble  $\nabla \cdot \mathbf{v}_\theta = 0$ . Therefore, the radial part of the velocity is the only contributor to the density variations.
- [28] N. Oppenheimer, D. B. Stein, M. Y. Ben Zion, and M. J. Shelley, *Nature Communications* **13**, 804 (2022), arXiv:2103.00296.
- [29] A. Ashkin, *Physical Review Letters* **24**, 156 (1970).
- [30] M. Y. Ben Zion, Y. Caba, A. Modin, and P. M. Chaikin, *Nature Communications* **13**, 184 (2022), arXiv:2012.15087.
- [31] M. Y. Ben Zion, A. Modin, and P. M. Chaikin, *Arxiv cond-mat.soft* (2022), doi.org/10.48550/arXiv.2203.11051, arXiv:2203.11051.
- [32] M. Doi, *Soft Matter Physics* (Oxford University Press, Oxford, 2013) p. 272.
- [33] C. P. Kelleher, A. Wang, G. I. Guerrero-García, A. D. Hollingsworth, R. E. Guerra, B. J. Krishnatreya, D. G. Grier, V. N. Manoharan, and P. M. Chaikin, *Physical Review E - Statistical, Nonlinear, and Soft Matter Physics* **92**, 1 (2015), arXiv:1701.08801.